Assessment of iterative image reconstruction techniques for small-animal PET imaging applications

E.Karali, S. Pavlopoulos, and D. Koutsouris

Abstract— **The purpose of this study is to assess the performance of iterative reconstruction methods, using phantom data from a prototype small-animal PET system. The algorithms compared are the simultaneous versions of ART (SART), EM-ML, ISRA WLS and a new iterative algorithm we have introduced under the short name ISWLS. The evaluation study was based on reconstructed image quality, as it is derived from visual inspection, cross-correlation coefficient and CNRs (contrast-to-noise ratios) of specific ROIs (region-of-interest). In general EM-ML and ISRA present similar reconstruction time and minor differences in reconstructed image quality. Slightly superior performances show WLS and SART while ISWLS improves reconstruction resolution at the edges of the field of view.**

I. INTRODUCTION

Small animal imaging is the conjunctive ring between experimental research and clinical implementation. Positron Emission Tomography (PET) has proven a valuable tool for in vivo small animal functional imaging. Such studies require imaging systems with spatial resolution less than 2 mm and high sensitivity in order to monitor radioisotopes of small specific activity [1][2].

A small-animal PET scanner dedicated to high resolution imaging of small laboratory animals has been recently developed by researchers in Spain [3] . This tomograph is a fully three-dimensional (3D) PET system based on two rectangular LYSO ($Lu_{0.6}Y_{1.4}SiO_{0.5}Ce$) detectors. The scanner displays a spatial resolution of 1.2 mm full-width at half maximum (FWHM) [3].

Image reconstruction in PET uses the collected projection data of the object/patient under examination. Until recently, image reconstruction in commercial clinical PET systems has been performed with analytical reconstruction algorithms, based on Filtered BackProjection method (FBP). Analytical techniques present high computational speed at low computational cost and in general do not require expensive, powerful computing systems. One of the major drawbacks of FBP methods is their lack to incorporate in the reconstruction process many of the different factors related to γ-ray production and detections and other factors affecting image quality (e.g. system geometry, object and septa scatter, detector characteristics, positron range, photons non-colinearity, randoms, photon attenuation). Moreover FBP does not preserve image non-negativity while the effect of missing data tends to produce streak artefacts in the reconstructed images [1].

Iterative image reconstruction algorithms have been proposed as an alternative to conventional analytical methods. Despite their computational complexity, they become more and more popular mostly because they can produce images with better contrast-to-noise (CNR) and signal-to-noise (SNR) ratios at a given spatial resolution compared to FBP techniques. Iterative methods are able to incorporate a model of all the physical phenomena during the acquisition process, including scanner characteristics. Based on predetermined criteria and after a series of successful iterations, they attempt, to find the best approach to the true image of radioactivity spatial distribution. The high computational cost and the lack of an efficient termination criterion have prevented, in the previous years, their application in commercial systems [1]. The only iterative algorithms that have recently been included in clinical PET systems software are two dimensional (2D) ordered subsets expectation maximization (OSEM) and three dimensional (3D) row-action maximum likelihood expectation maximization (RAMLA) [4].

The purpose of this study is to assess the performance of iterative reconstruction methods, using phantom data from a prototype small-animal PET system. The algorithms being compared are the simultaneous versions of ART (SART), EM-ML, ISRA and WLS and a new iterative algorithm we have introduced under the short name ISWLS. The methods presented here are applied to 2D sinograms.

.

II. THEORY

In general every iterative method relies on the hypothesis that the projection data **y** are linearly connected to the image **x** of radiopharmaceutical spatial distribution according to the equation:

$$y = A^T x \qquad (1)$$

where **A** is a matrix that characterizes the PET system being used for data acquisition. In bibliography this matrix is called system or probability matrix that projects image data to sinogram domain (the term sinogram refers to the projection data matrix). Every element $\alpha_{ij}$of the system matrix **A** represents the probability an annihilation event emitted in image pixel i is detected in LOR_j. The significance

E. Karali, S. Pavlopoulos and D. Koutsouris are with the National Technical University of Athens, Department of Electrical and Computer Engineering, Biomedical Engineering Laboratory, Athens, Greece. e-mail: ekarali@biosim.ntua.gr, spav@biomed.ntua.gr, dkoutsou@biomed.ntua.gr.

of the probability matrix lies on the valuable information regarding the data acquisition process that can contain (e.g. number of detector rings, ring diameter, number of detector elements in every ring, diameter of transaxial field of view, detector dimensions, image size, spatial and angular sampling).

The most commonly used algebraic simultaneous iterative method is SART [4] (Simultaneous Algebraic Reconstruction Technique) with updating scheme in k^{th} iteration:

$$\text{SART:} \quad x_i^k = x_i^{k-1} + \frac{\lambda_k}{\sum_{j=1}^{M} a_{ij}} \sum_{j=1}^{M} a_{ij} \frac{y_j - \sum_{i'=1}^{N} a_{i'j} x_{i'}^{k-1}}{\sum_{i'=1}^{N} a_{i'j}} \qquad (2)$$

The relaxation parameter in Eq. (3) $\lambda_k \in (0,1]$.

On the other hand the most commonly used least squares algorithms that are based on simultaneous iterative schemes are ISRA [6] (Image Space Reconstruction Algorithm) and WLS [7] (Weighted Least Squares) with updating step in k^{th} iteration:

$$\text{ISRA:} \quad x_i^k = x_i^{k-1} \frac{\sum_{j=1}^{M} a_{ij} y_j}{\sum_{j=1}^{M} a_{ij} \sum_{i'=1}^{N} a_{i'j} x_{i'}^{k-1}} \qquad (3)$$

$$\text{WLS:} \quad x_i^k = x_i^{k-1} \sum_{j=1}^{M} \frac{a_{ij} y_j^{\,2}}{\left(\sum_{i'=1}^{N} a_{i'j} x_{i'}^{k-1} \right)^2} \qquad (4)$$

Expectation Maximization Maximum Likelihood (EM-ML) algorithm [8] has an updating step in k^{th} iteration:

$$\text{EM-ML:} \quad x_i^k = x_i^{k-1} \sum_{j=1}^{M} \frac{a_{ij} y_j}{\left(\sum_{i'=1}^{N} a_{i'j} x_{i'}^{k-1} \right)} \qquad (5)$$

In the current work, we are proposing a new algorithm under the short name ISWLS, which has an updating step in k^{th} iteration:

$$\text{ISWLS:} \quad x_i^k = x_i^{k-1} \frac{\sum_{j=1}^{M} a_{ij} y_j^2}{\sum_{j=1}^{M} a_{ij} \sum_{i'=1}^{N} \left(a_{i'j} x_{i'}^{k-1} \right)^2} \qquad (6)$$

III. SYSTEM DESCRIPTION

A. System Configuration

Fig. 1 presents the basic schematic diagram of the prototype small animal PET system. The PET scanner consists of two rectangular LYSO ($Lu_{0.6}Y_{1.4}SiO_{0.5}Ce$) detectors, 44.8 mm × 44.8 mm × 12 mm in size. The two detectors are 160mm apart. Each of them is pixelized in 28 × 28 crystal cells, and each crystal cell is 1.6 mm × 1.6 mm × 1.2 mm in size. These planar detectors are attached to a gantry with rotation range 0^o-180^o.

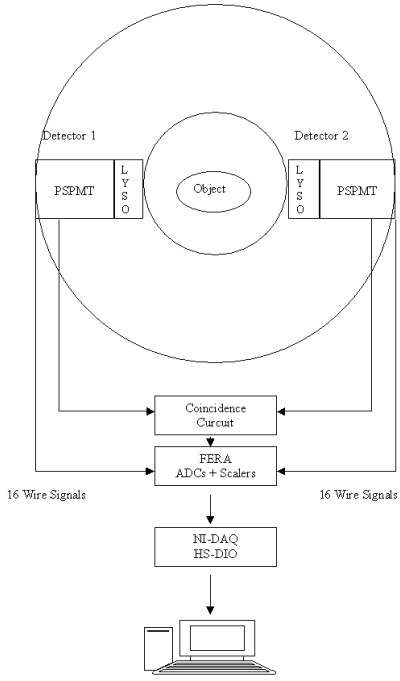

Fig.1. A schematic view of the prototype small-animal PET system

Cerium-doped lutetium-yttrium oxyortho-silicate (LYSO) is characterized by light yield comparable to LSO with slightly longer decay time of 53ns [9]. It is a variant of LSO in which some of the lutetium is replaced by yttrium atoms and has recently been developed at CTI Inc. in order to be used in phoswich detector architectures. The properties of LYSO in comparison to LSO, BGO and GSO are summarized in Table I.

TABLE I: PROPERTIES OF MOST COMMON SCINTILATOR MATERIALS BEING USED IN PET SYSTEMS

	LYSO	LSO	GSO	BGO
Decay time (ns)	53	40	60/600	60/300
Light output (PMT)	75	75	20	15
Light output (APD)	85	85	40	30
Peak emission (nm)	420	420	430	480
Index of refraction	1.81	1.82	1.85	2.15
Density (g/cm^3)	5.37	7.35	6.71	7.13
Effective Z	54	65	58	73
$1/\mu$ (mm) (511 keV)	20	12.3	15	11.6

Every scintillator is coupled to a Position Sensitive Photomultiplier Tube (PSPMT Hamamatsu R3941). We have built a special hardware configuration for coincidence detection and real-time data acquisition, which is performed by a PC. The coincidence data are then reconstructed off-line

using specific software written in C++ (Borland Builder 6). The spatial resolution of the system is about 1.2 mm [3].

B. Data Acquisition

The line that connects the centers of two antidiametrical detector pixels defines a projection line of response (LOR). Between two adjacent LORs a detector tube-of-response (TOR) is formed. Every detector consists of 28×28=784 pixels, so the detection system could be consider having 28 partial rings of 56 detectors in each ring. This means that every ring contains two rotating blocks of 28 detectors each. The system operates in 2D and 3D acquisition modes. In 2D mode only coincidences between detectors of the same ring are allowed. So for every angle in the 2D sinogram data from 55 LORs are collected. In 3D mode data is binned into 28 direct and 756 (28^2-28) oblique 2D sinograms.

IV. RESULTS

For the evaluation of the iterative reconstruction methods, presented in Section II, projection data of a Derenzo-type phantom has been used. The Derenzo-type phantom was constituted by sets of rods, filled with F^{18}, with diameters 4.8, 4, 3.2, 2.4, 1.6, and 1.2 mm, and the same separation between surfaces in the corresponding sets. The rods were surrounded with plastic (polyethylene).

The data were acquired with the prototype small-animal PET scanner, described in Section III. 18×10^6 coincidence events were collected. Projection data was binned to a 2D sinogram, $55\text{pixels} \times 170$ pixels in size, which means that data from 55 TORs per rotation angle were collected and 170 totally angular samples were used. Since the two detector heads rotate from 0^o to 180^o the angular step size was 1.058^o.

The system matrix was derived from an analytical method and calculated once before reconstruction. Each element a_{ij} was computed based on the area of intersection E_{ij} ,of TOR_j with image pixel i, according to the equation:

$$a_{ij} = \frac{E_{ij}}{\sum_{j=1}^{M} E_{ij}} \tag{7}$$

where M is the number of sinogram elements ($M=55 \times 170$). The calculated system matrix is a sparse matrix. It consists of zero valued elements in majority that have no contribution during iterative reconstruction process. So, only the non-zero elements were stored with significant reduction in system matrix size and as a result in required storage, as well. Fig. 2 shows the variation of system matrix sparsity (in percentage) with increasing image size (in pixels). The reconstructed 2D images were $128\text{ pixels} \times 128$ pixels in size, thus the system matrix consisted of $55 \times 170 \times 128 \times 128$ elements with 4.33% sparsity.

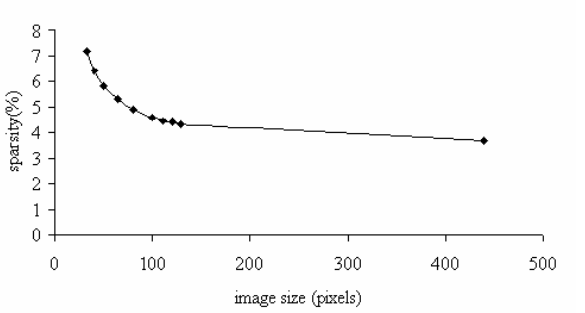

Fig.2. The variation of system matrix sparsity (in percentage) with increasing image size

The initial image estimate for EM-ML, ISRA, WLS and SART was:

$$x_{o_i} = \frac{\sum_{j=1}^{M} y_j}{N^2}, \quad \text{i} = 1,2,..., \text{N} \tag{8}$$

where y_j is the value of the j^{th} sinogram element and N^2 represents the total number of image pixels (N=128 in this implementation).

Fig. 3 shows the reconstructed transaxial images with EMML, ISRA, WLS, ISWLS and SART after 10, 50 and 100 iterations.

In Fig. 4 cross-correlation coefficient c of every iterative method is plotted versus the number of iterations. The cross-correlation coefficient c was calculated according to the equation:

$$c = \frac{\sum_{i=1}^{N}\sum_{j=1}^{N}\left(Irecon_{ij} - \bar{I}recon\right)\left(Ireal_{ij} - \bar{I}real\right)}{\sqrt{\sum_{i=1}^{N}\sum_{j=1}^{N}\left(Irecon_{ij} - \bar{I}recon\right)^2 \sum_{i=1}^{N}\sum_{j=1}^{N}\left(Ireal_{ij} - \bar{I}real\right)^2}} \tag{9}$$

where $\bar{I}recon$ and $\bar{I}real$ are the reconstructed image and the true phantom activity image mean values, respectively. Cross-correlation coefficient consists of a similarity measure between reconstructed and real radiodistribution image. Its values are in the range of [-1, 1]. Value c=1 corresponds to fully correlated images [10].

Except from cross-correlation coefficient that shows the reconstruction methods average performance, local contrast-to-noise ratios (CNR) for rods with different diameters were calculated. CNRs for 4.8, 3.2, and 1.6 mm rods diameter were computed using squared regions-of-interest (ROIs), 4.55, 3.85 and 2.15 mm in size, respectively. The ROIs were placed inside the corresponding objects. The number of selected ROIs was equal to the number of same sized objects. ROIs of the same sizes were positioned in three different background areas, for every case. CNR_{ROI} was

defined as: $$CNR_{ROI} = \frac{R_{obj_{ROI}} - R_{Backg_{ROI}}}{\sigma_{Backg_{ROI}}} \quad (10)$$

where $R_{obj_{ROI}}$ is the mean value of reconstructed objects in the corresponding ROIs and $R_{Backg_{ROI}}$ is the mean value of the three background ROIs in each case.

$\sigma_{Backg_{ROI}}$ is the standard deviation of background values in the corresponding ROIs. The graphs in Fig. 5 illustrate the variation of CNR_{ROI} with respect to the number of iterations, for the three different objects diameters

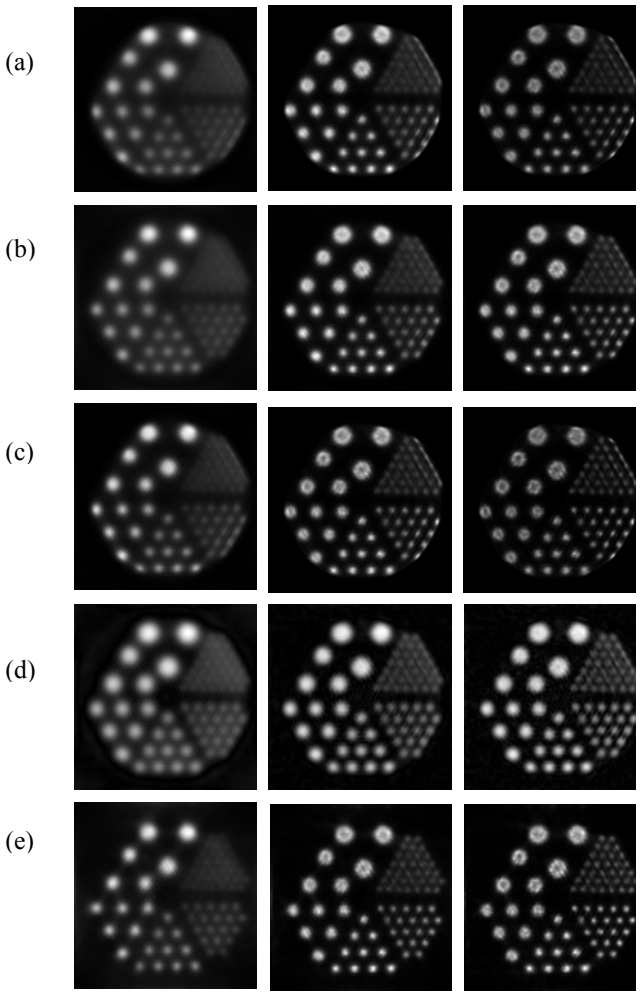

Fig.3. Reconstructed images with a) emml, b) isra, c) wls, e) sart και f) iswls after 10, 50 and 100 iterations respectively

.

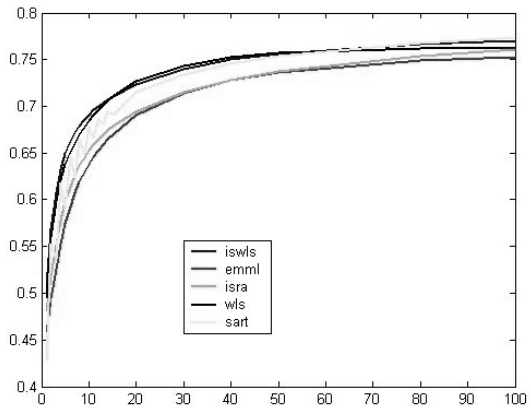

Fig.4. Cross-correlation coefficient versus the number of iterations for

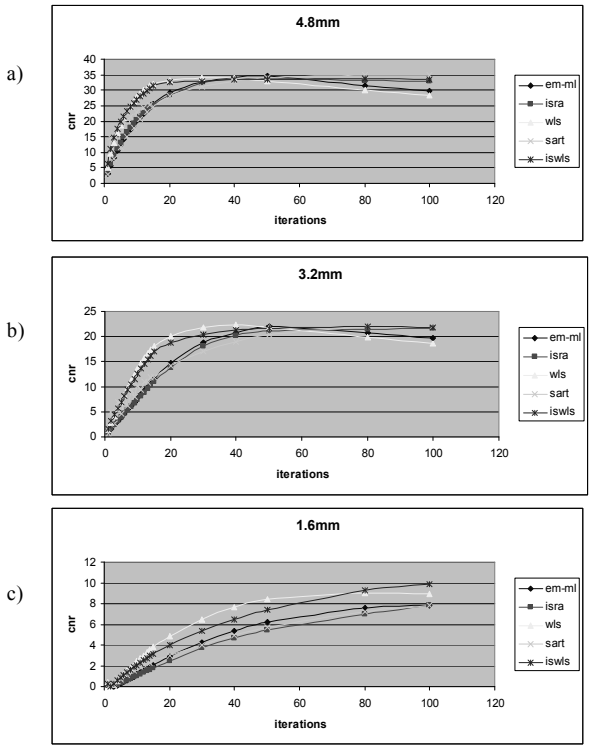

Fig.5. CNRs versus iterations for a) 4.8mm, b) 3.2mm and c) 1.6mm object diameter

In Fig.6 the reconstruction time for every iterative algorithm is presented as a function of the number of iterations. Reconstruction time calculations were performed on a Pentium M processor 1400 MHz (Intel Corp.) personal computer (RAM 1280MB) under Windows XP Professional.

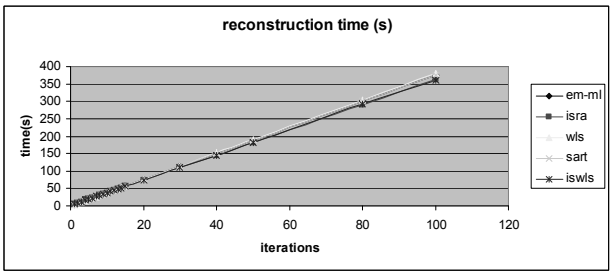

Fig.6. Reconstruction time/slice as a function of the number of iterations

V. DISCUSSION

All the algorithms achieve high cross-correlation values as the number of iterations increases. Cross-correlation coefficients of EM-ML and ISRA present almost the same variance as a function of the number of iterations. Reconstructed images with SART, WLS and ISWLS achieve high correlation levels with the real radiodistribution image after the first 10 iterations. As the number of iterations outreaches 90 to 95 cross-correlation of all iterative algorithms converges to the same value.

As it is illustrated in Fig. 5 EM-ML converges slowly during the first 50 iterations to the best approximation of the true image. After the 50 iterations the algorithm enhances more image detail (small sized objects). However after that point image contrast decreases, while noise component starts to increase. On the contrary ISRA, in comparison to EM-ML, presents better performance between 50-100 iterations where it reaches relatively high and constant CNRs values for big and small sized image objects. WLS shows almost identical noise manipulation as the EM-ML. Image contrast starts degrading after 50 iterations due to increasing noise. On the other hand WLS reaches same CNR values faster than EM-ML in the first iterations. SART performance is a compromise between EM-ML, ISRA and WLS during the first 50 iterations. CNRs of both small and big image objects achieve adequate values (CNR>3-5, Rose Criterion [11]) while still increasing during the first 100 iterations. However partial volume effect is more obvious in SART than the other reconstruction algorithms, which may be the reason for the low CNRs values, in comparison to WLS. ISWLS presents high CNR ratios from the first iterations. Although it shows similar performance to WLS it's CNR ratios do not degrade after 50 iterations but tend to be stabilized. Moreover it improves reconstruction resolution at the edges of the field of view.

Reconstruction time of EM-ML, WLS and SART are almost the same as a function of the number of iterations ($\approx$3.8s/iteration). Although it is not obvious from Fig. 6, ISRA and ISWLS are slower than EM-ML, WLS and SART during the first 9 iterations. Its reconstruction speed is gradually improving with increasing number of iterations. ISWLS and ISRA reconstruction time converges to the others after 10 iterations. The reason for slow reconstruction process during the first iterations lies on the time needed for backbrojection computations ($\sum_{i=1}^{M} a_{ij} y_j$ for ISRA and $\sum_{i=1}^{M} a_{ij} y_j^2$ for ISWLS) in the first iteration.

VI. CONCLUSION

In this work different simultaneous iterative reconstruction schemes were applied to data acquired from a prototype small-animal PET scanner. SART, and EM-ML, ISRA, WLS and ISWLS iterative algorithms were implemented and evaluated in terms of task-dependent measures for quantization and detection. In general EM-ML and ISRA present similar reconstruction time and minor differences in reconstructed image quality. Slightly superior performances show ISWLS WLS and SART

REFERENCES

[1] M.E. Phelps, "PET Molecular Imaging and its Applications", New York: Springer-Verlag, 2004, ch. 1.

[2] Simon R. Cherry and Sanjiv S. Gambhir, "Use of Positron Emission Tomography in Animal Research", *ILAR Journal*, vol. 42, No 3, pp:219-231, 2001.

[3] J. E. Ortuno, P. Guerra-Gutierrez, J. L. Rubio, G. Kontaxakis, A. Santos, "3D-OSEM iterative image reconstruction for high resolution PET using precalculated system matrix", ITBS 2005.

[4] G. Tarantola, F. Zito, P.Gerundini, "PET Instrumentation and Reconstruction Algorithms in Whole-Bode Applications", *J Nucl Medicine*, Vol.44, No.5, pp:756-768, May 2003.

[5] M. Jiang and G. Wang, "Convergence Studies on Iterative Algorithms for Image Reconstruction", *IEEE Trans. Med. Imag.*, Vol 22, No 5, pp:569-579, May 2003.

[6] G.E.B. Archer and D.M. Titterington, "The Iterative Image Space Reconstruction Algorithm (Isra) as an alternative to the EM algorithm for solving Positive Linear Inverse Problems*", Statistica Sinica*, Vol 5, pp:77-96, 1995.

[7] M.M. Anderson, B.A. Mair, M. Rao and C.H. Wu, "Weighted Least-Squares Reconstruction Methods for Positron Emission Tomography", *IEEE Trans. Med. Imag*., Vol 16, No 2, pp: 159-165, April 1997.

[8] L.A. Shepp and Y. Vardi, "Maximum Likelihood Reconstruction for Emission Tomography", *IEEE Trans. Med. Imag.,* Vol MI-1, No 2, October 1982.

[9] C.M. Pepin, P. Bérard, A.L. Perrot, C. Pépin, D. Houde, R. Lecomte, C.L. Melcher and H. Dautet, "Properties of LYSO and Recent LSO Scintillators for Phoswich PET Detectors", *Trans. Nucl. Science,* vol. 51, No 3, pp:789-795, June 2004.

[10] E. Karali, P. Asvestas, K.S. Nikita and G.K. Matsopoulos, "Comparison of Different Global and Local Automatic Registration Schemes: An Application to Retinal Images ", Proceedings of MICCAI 2004, LNCS 3216 , Part 1, pp:813-820, Springer-Verlag Berlin Heidelberg, 2004.

[11] S.R. Cherry, J. A. Sorenson, M. E. Phelps, "Physics in Nuclear Medicine", SAUNDERS-Elsevier, 2003, ch. 15.